THE JOURNAL OF PHYSICAL CHEMISTRY C

Article

pubs.acs.org/JPCC

Optical Properties of Bilayer Graphene Nanoflakes

Marzio De Corato,*[,†,‡] Caterina Cocchi,[‡,∥] Deborah Prezzi,[‡] Marilia J. Caldas,[§] Elisa Molinari,[†,‡] and Alice Ruini*[,†,‡]

[†]Dipartimento di Scienze Fisiche, Informatiche, Matematiche, Università di Modena e Reggio Emilia, I-41125 Modena, Italy

[‡]Centro S3, CNR-Istituto Nanoscienze, I-41125 Modena, Italy

[§]Instituto de Física, Universidade de São Paulo, 05508-900 São Paulo, SP, Brazil

Supporting Information

ABSTRACT: The optical properties of coupled graphene nanoflakes are investigated theoretically within the framework of Hartree−Fock based semiempirical methods, with the aim of unraveling the role of $\pi-\pi$ interactions. Two different types of π-stacking are considered, obtained either by coupling two identical flakes with different relative displacement or by coupling flakes having different width or edge functionalization, i.e., with different electronic gap or ionization potential. Our results indicate that a systematic red shift and broadening of lowest excitations occur: an overall widening of the optical absorption range can therefore be expected in an ensemble of flakes. However, the coupling prevents a strong enhancement of the absorption intensity. In the case of a heterogeneous ensemble of flakes, the possibility of introducing low-energy excitations with considerable charge transfer character is also demonstrated by properly exploiting the chemical edge functionalization.

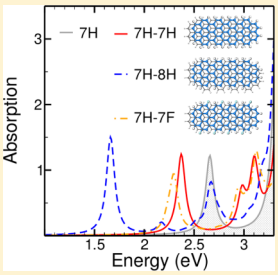

INTRODUCTION

Strong noncovalent interactions between π-conjugated systems are strategic in biochemistry, supramolecular chemistry, and materials science. In fact, they typically show up spontaneously and control such diverse phenomena as the vertical base−base interactions which stabilize the double helical structure of DNA,[1] the tertiary structures of proteins,[2,3] the aggregation of polycyclic aromatic hydrocarbons (PAHs),[4,5] and the aromatic molecules in organic crystals[6,7] and in discotic liquid crystals.[8,9] Because of their intriguing photoluminescence phenomena,[10,11] supramolecular π-stacked structures have particular technological relevance for optoelectronic applications.

More recently, the relevance of π-stacking emerged also in graphene[12−15] and its nanostructures,[16−18] such as graphene nanoribbons. The electronic and optical properties of isolated ribbons have been shown to be highly sensitive to the details of the atomic structure: the specific edge shape (armchair vs zigzag) implies different electronic and magnetic properties,[19−21] and even slight ribbon width variations induce striking modifications in the electronic and optical properties.[22−24] In addition, edge functionalization can also be exploited to modulate their properties even further.[25−29] While most previous studies were limited to isolated graphene nanostructures, the effect of $\pi-\pi$ interactions should be considered in view of the fact that they spontaneously occur (e.g., when graphene nanostructures are obtained in solution[30] or by unrolling multiwall carbon nanotubes[16,17]) and with the idea to intentionally exploit the layer stacking as an additional parameter to tune their electronic[31−36] and optical properties.[36,37]

We here focus on the effect of $\pi-\pi$ coupling on the optical properties of finite ribbons, i.e., elongated graphene nanoflakes (GNFs). Our study comprises several bilayer graphene nanoflakes (BGNFs), including both homogeneous stacking (different geometries for the π-stacking between two identical nanostructures) and heterogeneous stacking (π-stacking between two different nanostructures, namely, with different width or with different edge functionalization). For all considered coupled systems, we find that the low-energy optical excitations are red-shifted and broadened with respect to their isolated counterparts. A proper choice of edge functionalization is also demonstrated to give rise to charge-transfer excitations. Our whole analysis confirms that the $\pi-\pi$ coupling impacts the optical properties of GNFs, and it can also provide an efficient strategy to shape the optical properties of such low-dimensional nanostructures.

COMPUTATIONAL DETAILS

We investigate a number of bilayer structures, composed of elongated GNFs with armchair edges along the length; the flake ends are shaped to minimize the zigzag region and thus to avoid spin-related effects.[38,39] The bilayer systems are built by stacking two identical flakes (homogeneous stacking), as shown in Figure 1, or two flakes differing from each other by either width or edge functionalization (heterogeneous stacking); see Figure 3. In the following, single and bilayer systems are labeled according to both their width parameter N,[40] which indicates the number of dimers along the zigzag direction (y axis in Figure 1), and their edge terminations. According to this notation, we consider the homogeneously stacked 7H-7H

Received: April 30, 2014
Revised: August 27, 2014
Published: September 9, 2014

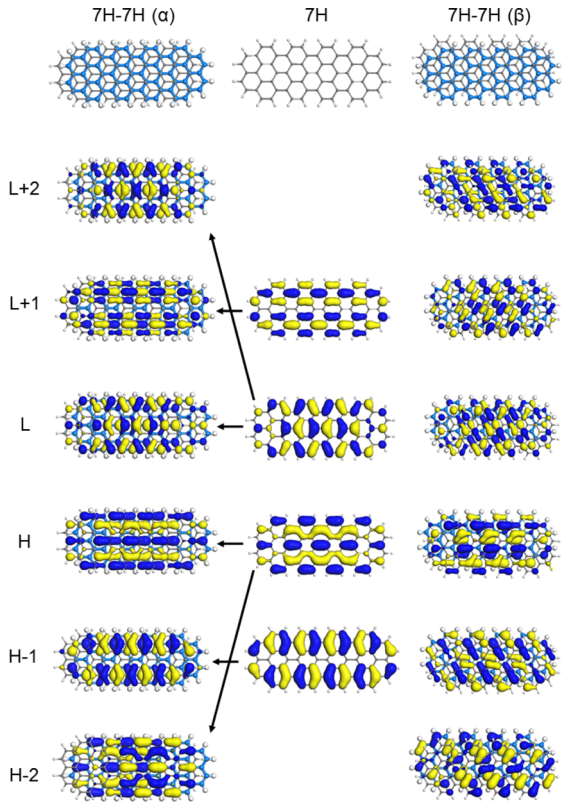

Figure 1. Ball-and-stick models of the 7H GNF and the 7H-7H BGNFs (upper panel), with their related frontier orbitals. The bilayer structures are obtained by combining two $N = 7$ GNFs in Bernal stacking with different displacements, i.e., α (left panel) and β (right panel); see text. C atoms of the top (bottom) layer are in gray (blue); H atoms are in white. The frontier orbitals are also shown for the single GNF (central panel): for the α stacking the derivation of the BGNF orbitals from the ones belonging to the individual GNF is evident and highlighted with arrows.

BGNF, which is obtained by coupling two hydrogen terminated GNFs with $N = 7$, hereafter labeled 7H; the heterogeneously stacked 7H-8H and 7H-7F BGNFs, which are obtained by coupling the 7H GNF with the hydrogenated $N = 8$ one (8H) and with the edge-fluorinated $N = 7$ one (7F).[41]

The optical properties are computed within the framework of the Hartree−Fock based semiempirical ZINDO method,[42] which is well-tested and reliable for the study of C-conjugated low-dimensional systems[43−48] also in nonbonded $\pi-\pi$ intermolecular conformations.[49] The AM1 model,[50] usually adopted for structural optimization of covalently bonded molecular systems, is however not designed to capture the effect of intermolecular (van der Waals) interactions. Hence, we performed geometry optimizations by means of first-principles density-functional theory (DFT) calculations by using plane-waves basis set, ultrasoft pseudopotentials, the Perdew−Burke−Ernzerhof exchange correlation functional,[51] and van der Waals interactions through the semiempirical DFT-D2 approach by Grimme,[52] as implemented in the Quantum ESPRESSO package.[53] This approach has proven successful for the description of several C-based materials[54] and is employed here for both single and bilayer systems.[55] The plane-wave kinetic-energy cutoff was set to 30 Ry for the wave functions and 240 Ry for the charge density for hydrogen-terminated GNFs and increased to 48 and 384 Ry, respectively, for systems including F. Structures were relaxed using a threshold for the forces on atoms of 10^{-4} Ry/au.

Starting from the DFT-D2 geometries, optical spectra are evaluated by employing the semiempirical ZINDO/S approach with single excitation configuration interaction (CIS).[56] Our convergence tests over the number of occupied and virtual molecular orbitals (MOs) indicate that a CI energy window of at least 4.5 eV below the HOMO and 3.5 eV above the LUMO is required for a reliable characterization of the low-energy optical excitations.

To further analyze the nature of the main optical excitations, we compute the spatial distribution of their electron (e) and hole (h) components, as described in ref 57. Starting from the MOs in the standard LCAO expansion[58]

$$\phi_i(\mathbf{r}) = \sum_j a_{ji}\chi_j(\mathbf{r}) \tag{1}$$

where $\chi_j(\mathbf{r})$ are Slater-type orbital basis functions and a_{ji} are the projection coefficients, the probability density of h and e for the Ith excited state can be expressed as

$$\rho_{\mathrm{h}}^{I}(\mathbf{r}) = \sum_{\alpha\beta} |c_{\alpha\beta}^{I}\cdot\phi_\alpha(\mathbf{r})|^2 \tag{2}$$

$$\rho_{\mathrm{e}}^{I}(\mathbf{r}) = \sum_{\alpha\beta} |c_{\alpha\beta}^{I}\cdot\phi_\beta(\mathbf{r})|^2 \tag{3}$$

Here $c_{\alpha\beta}^{I}$ are CI coefficients weighting the contribution to the Ith excitation of each transition $\alpha \rightarrow \beta$ from occupied (ϕ_α) to virtual (ϕ_β) MOs. The spatial localization of the excitation can then be quantified by integrating $\rho_{\mathrm{e/h}}^{I}(\mathbf{r})$ over a selected region of the total system.[57]

RESULTS AND DISCUSSION

Homogeneous Stacking. We first consider a system composed of two identical hydrogenated $N = 7$ (7H) GNFs. As shown in Figure 1, two different arrangements of the 7H flakes can be identified as compatible with the Bernal stacking typical of graphite, which we label as 7H-7H(α) and 7H-7H(β), following the notation of refs 36 and 59. In the α stacking (Figure 1, upper left panel), one flake is shifted with respect to the other by a single C−C bond length along the x direction; in the β stacking the same displacement is applied along a direction forming an angle of $\pi/3$ with the x axis (Figure 1, upper right panel). The interlayer distance is almost identical for the α and β arrangements (3.310 and 3.312 Å, as evaluated at the flake center), and the α configuration is slightly more stable than the β one (by 0.01 eV). The different packing conformations result mostly in different alignments of the flake edges (see Figure 1), which give rise to different combinations for the molecular orbitals of the BGNFs.

The absorption spectra of the 7H-7H BGNFs for both α and β stackings are shown in Figure 2a, as compared to the spectrum of the single 7H GNF. The interlayer coupling clearly produces a red shift of the first absorption peak of about 0.30 eV for the α stacking and 0.15 eV for the β stacking. Analyzing the one-electron level structure (Figure 1), we see that in both cases the HOMO and LUMO of the bilayer are related to a level splitting that is connected, respectively, to the HOMO and LUMO of the individual flakes. However, while the α stacking preserves the yz reflection symmetry, this is not the case for the β stacking. The different symmetry results in different energy splittings for α and β, similar to the case of

dx.doi.org/10.1021/jp504222m | J. Phys. Chem. C 2014, 118, 23219−23225

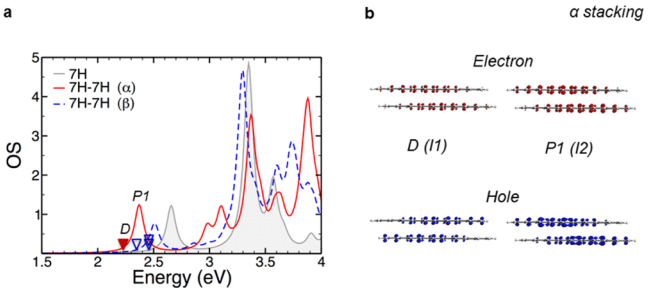

Figure 2. Optical properties of the 7H-7H BGNFs. (a) Absorption spectra for the α (solid red) and β (dashed blue) stacking configurations, compared to the spectrum of the isolated $N = 7$ GNF (gray area). Triangles indicate optically inactive states. For the spectra we use a Lorentzian broadening of 100 meV. (b) Probability densities of the electrons (red) and holes (blue) for the first dark (D) and the first optically active (P1) excitation of the 7H-7H (α) BGNF (D and P1 are also indicated as I1 and I2, according to the notation in Table 1).

infinite bilayer nanoribbons of the $3p + 1$ family.[36] The first optically active excitation (P1) for both α and β configurations is mainly composed of the HOMO → LUMO transition (H → L; see Table 1) and is thus directly derived from that of the single 7H flake. As the HOMO and LUMO orbitals of the BGNFs are homogeneously distributed over the single flakes (see Supporting Information and Figure 1, left panel), the e and h probability densities for this excitation are equally distributed over the two flakes (see Figure 2 for the α stacking).

Table 1. Low Energy Optical Excitations (I) of the 7H-7H (α) BGNF[a]

I	E	OS		$c_{\alpha\beta}^2$	$\mu_\parallel$	$\mu_\perp$
1	2.28	0.00	(0.52)	H − 1 → L	0.00	0.00
			(0.25)	H → L+1		
2	2.37	1.22	(0.83)	H → L	11.46	1.95
3	2.44	0.00	(0.14)	H − 4 → L	0.40	0.01
			(0.22)	H − 1 → L + 2		
			(0.33)	H → L + 3		
4	2.54	0.00	(0.35)	H − 2 → L	0.00	0.00
			(0.52)	H → L + 2		
20	3.37	2.97	(0.51)	H − 2 → L + 2	15.15	1.71
			(0.23)	H − 1 → L + 1		

[a]Energy (E, in eV), oscillator strength (OS), squared CI coefficients ($c_{\alpha\beta}^2$) of relevant transitions ($c_{\alpha\beta}^2 \geq 0.1$), and the projections of the transition dipole moment (μ in D) in the GNF plane (xy plane, $\mu_\parallel$) and perpendicular to it (z direction, $\mu_\perp$).

For both configurations, dark excitations are detected below the first optically active peak, as indicated by triangles in Figure 2a. Again, as for the isolated 7H GNF, they are mainly composed of H − 1 → L and H → L + 1 transitions (see Table 1 for the α stacking and Table S1 in Supporting Information for the β stacking). Indeed, the HOMO − 1 and LUMO + 1 states of the BGNFs are directly related to the splitting of the HOMO − 1 and LUMO + 1 levels of the single flake (see Figure 1). However, while for the α stacking we see only one dark state in this energy region (red triangles in Figure 2), in the case of β stacking three dark states (blue empty triangles) are found, as a consequence of the lower symmetry and different level splittings.

We thus see that a very small difference in the stacking configuration can produce a significant difference in the optical properties. Going further in this investigation, we found that, preserving the symmetry of the α stacking but imparting larger shifts between the GNFs in the x direction, the interlayer coupling weakens and finally vanishes because of insufficient π-overlap area (see Figure S2). In other words, the π-stacking in a realistic ensemble of identical flakes is expected to produce a significant broadening of the low-energy absorption peak, which can be about 0.4 eV for such subnanometer narrow flakes (as evaluated from the energy spread of the lowest peaks in the absorption spectra of differently coupled 7H flakes; see Figure 2).

On the other hand, even if one could expect a strong enhancement of the absorption intensity as compared to the single flakes, this is not the case because of the specific character of the transition dipole moment $\vec{\mu}$ in these GNFs: while $\vec{\mu}$ gains a small intensity in the direction normal to the flakes in the bilayer structures, there is a "ring-by-ring" cancellation in the parallel direction that compensates for the presence of two flakes.

Heterogeneous Stacking. After the homogeneous stacking of identical hydrogenated flakes, we now analyze the coupling of two hydrogenated flakes of different width, namely, $N = 7$ and $N = 8$, resulting in the 7H-8H BGNF displayed in Figure 3a. In Figure 3b we show the AM1 electron affinities and ionization potentials calculated for the isolated flakes. The smaller gap associated with the 8H flake, as expected from the $3p + m$ modulated electronic properties of GNFs,[57,60] suggests that the low-energy optical activity of the bilayer structure will be dominated by the excitations of the 8H flake, as we will confirm in the following.

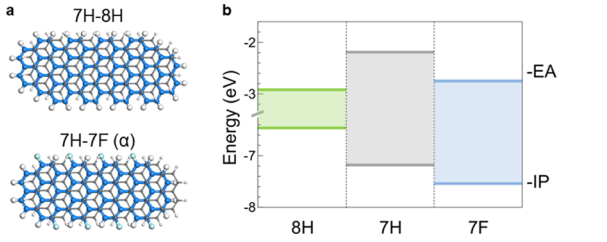

Figure 3. (a) Ball-and-stick model of the 7H-8H and 7H-7F BGNFs. C atoms of the 7H GNF are in gray, and C atoms of the 8H and 7F GNFs are in blue. H atoms are in white and F atoms in light blue. (b) Scheme for the electron affinity (EA) and ionization potential (IP) of the single GNFs considered here, calculated using the AM1 method (see text).

The frontier orbitals of the 7H-8H BGNF (see Figure S1, central panel) are consistent with the level alignment displayed in Figure 3b: we find that the HOMO and LUMO states are mainly localized on the 8H flake, while HOMO − 1 and LUMO + 1 are more localized on the 7H flake. The optical spectrum of the 7H-8H BGNF, shown in Figure 4a, reflects this spatial separation of the frontier orbitals: at first sight, it indeed looks like a simple superposition of the spectra of the individual 7H and 8H GNFs. In fact, the first active excitation P1 derives from the first excited state of the 8H flake, since it is mainly composed of the H → L transition and therefore prevalently localized on the 8H flake, as also shown by the corresponding e/h densities in Figure 4b. Furthermore, the second most prominent peak P3, mainly involving the H − 1 → L + 1 transition, is accordingly more localized on the 7H GNF, thus

dx.doi.org/10.1021/jp504222m | J. Phys. Chem. C 2014, 118, 23219−23225

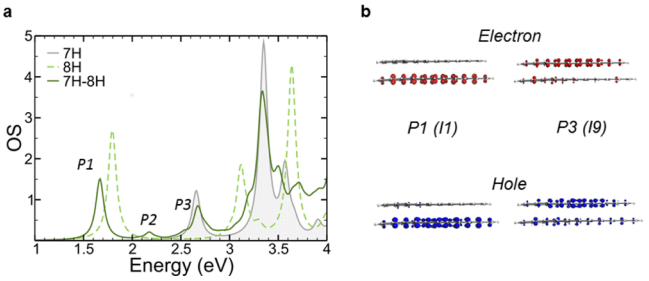

Figure 4. (a) UV−vis spectrum of the 7H-8H BGNF (solid dark green) compared to the spectra of the isolated 7H (gray area) and 8H GNFs (dashed light green). The spectra are obtained by using a Lorentzian broadening of 100 meV. (b) Electron (red) and hole (blue) probability densities for the two main low-energy peaks P1 and P3, indicated in (a) and labeled as *I*1 and *I*9 in Table 2.

retaining the character of the first peak of the 7H GNF, as shown by the e/h densities in Figure 4b. Nonetheless, some subtle features can be directly related to the $\pi-\pi$ coupling between the two flakes, such as the lowering of the oscillator strengths (dipole effect), the slight energy shifts of the main peaks (interaction splitting), and the appearance of other low-energy excitations, such as the new peak P2 at intermediate energy in Figure 4 (corresponding to the *I*3 excitation in Table 2), for which the e/h density is in fact almost equally

Table 2. Low Energy Optical Excitations (I) of the 7H-8H BGNF[a]

I	E	OS	$c_{\alpha\beta}^2$		$\mu_\parallel$	$\mu_\perp$
1	1.66	1.49	(0.89)	H → L	15.36	0.92
2	2.06	0.02	(0.20)	H − 2 → L	1.55	0.06
			(0.31)	H − 1 → L		
			(0.11)	H → L + 1		
			(0.10)	H → L + 3		
3	2.17	0.17	(0.11)	H − 2 → L	4.16	1.74
			(0.45)	H − 1 → L		
			(0.32)	H → L + 1		
9	2.66	0.64	(0.44)	H − 1 → L + 1	7.96	0.30
			(0.12)	H → L + 2		
28	3.32	2.18	(0.10)	H − 2 → L + 1	13.12	0.90
			(0.10)	H − 1 → L + 3		

[a]Energy (E, in eV), oscillator strength (OS), squared CI coefficients ($c_{\alpha\beta}^2$) of relevant transitions ($c_{\alpha\beta}^2 \geq 0.1$), and the projections of the transition dipole moment (μ, in D) in the GNF plane (xy plane, $\mu_\parallel$) and perpendicular to it (z direction, $\mu_\perp$).

distributed over the two flakes, as shown in Figure S3. Combining the results of homogeneous and heterogeneous stacking of hydrogenated flakes, we confirm the conclusion that in a more disordered medium, the optical absorption range is expected to be expanded by over 1 eV.

We next consider the case of a heterogeneous bilayer structure obtained by means of different edge functionalization of the components, namely, the 7H-7F BGNF. Here we focus only on the α configuration, since we find that the differences between α and β alignment are very similar to those discussed for the fully hydrogenated case. As found for single fluorinated GNFs,[60] distortion effects appear also in the bilayer structure: they are mainly localized at the fluorinated edges and are even reduced compared to the isolated system, stating the relevance of intermolecular interactions.

From the scheme of the electron affinity and ionization potential of the individual flakes in Figure 3b, one could expect a corresponding sizable reduction of the optical gap in the BGNF with respect to the single flakes. Indeed, the energies of the first excited states (dark and active, D and P1, respectively) are downshifted by about 0.3 eV with respect to the 7H GNF (see Figure 5a). However, these excitation energies are almost

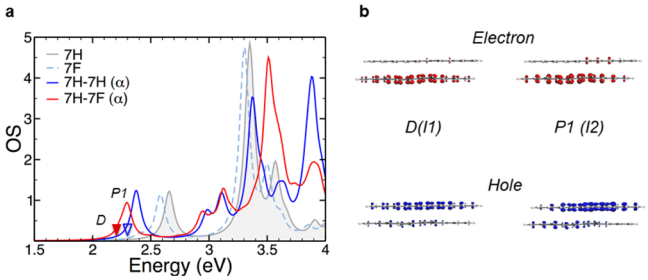

Figure 5. (a) UV−vis spectrum of the 7H-7F BGNF in α alignment (solid red) compared to the spectra of the isolated 7H (gray area) and 7F (dashed light blue) GNFs and of the 7H-7H BGNF (solid blue). For the spectra we use a Lorentzian broadening of 100 meV. The triangles indicate the position of dark states. (b) Electron (red) and hole (blue) probability densities of the first two excitations D and P1 (labeled as *I*1 and *I*2 in Table 3 for the 7H-7F(α) BGNF).

unchanged if compared to the homogeneous 7H-7H(α) stacking (Table 3 and Table 1). This is also the case for the β stacking, as detailed in the Supporting Information. Apparently, the interaction splitting leading to the gap closure in the fully hydrogenated BGNF equals the level alignment effect, which should dominate in the case of the heterogeneous 7H-7F stacking. Analyzing the localization of the frontier orbitals (see Figure S1, right panel), we find that although the LUMO and the LUMO + 1 are mainly localized on the 7F flake, the HOMO and the HOMO − 1 spread over both flakes (the latter to a smaller extent), indicating a sizable rehybridization of the states. This means that the reduction of the optical gap in the 7H-7F case is not only due to the type II level alignment but also due to interaction splitting effects. Furthermore, we can analyze the charge-transfer character of the lowest energy excitations. To this end, we compute the electron spatial localization of the Ith excitation L_e^I, integrating ρ_e^I over a box containing each of the flakes composing the bilayer structure, and analogously for the hole spatial localization L_h^I (see Table 3). We quantify the charge-transfer character of the excitation by computing the difference between electron and hole localization on the same flake. This analysis clearly highlights the difference between the 7H-7H and the 7H-7F systems: in the latter case the hole is mostly localized in the hydrogenated and the electron in the fluorinated flake for the lowest-energy excitations, which present a considerable charge transfer character (see Table 3 and Figure 5b). These results imply that in the case of a mixed ensemble of π-stacked flakes with different width and edge termination, the red shift and widening of the optical absorption range will be accompanied by additional charge transfer effects (similar effects were suggested for different π-coupled systems, e.g., like nanopeapods[61]).

CONCLUSIONS

We studied the effect of π-stacking on the optical properties of elongated graphene nanoflakes with armchair edges. Our study

dx.doi.org/10.1021/jp504222m | J. Phys. Chem. C 2014, 118, 23219−23225

Table 3. Low Energy Optical Excitations (I) of the 7H-7F (α) BGNF[a]

I	E	OS		$c_{\alpha\beta}^2$	$\mu_{\parallel}$	$\mu_{\perp}$	L_e^{7F}	L_h^{7F}	CT
1	2.24	0.17	(0.29)	H − 1 → L	4.39	0.74	0.78	0.36	0.42
			(0.14)	H → L					
			(0.27)	H → L + 1					
2	2.30	0.85	(0.71)	H → L	9.65	2.07	0.75	0.35	0.40
3	2.41	0.00	(0.20)	H − 1 → L + 2	0.80	0.14	0.50	0.38	0.12
			(0.11)	H → L + 3					
			(0.19)	H → L + 4					
4	2.50	0.05	(0.29)	H − 2 → L	2.37	0.43	0.45	0.40	0.05
			(0.51)	H → L + 2					
5	2.61	0.01	(0.10)	H − 2 → L + 1	1.26	0.00	0.74	0.38	0.36
			(0.20)	H − 1 → L					
			(0.23)	H → L + 1					
27	3.51	3.50	(0.25)	H − 4 → L + 1	16.20	0.43	0.60	0.44	0.16
			(0.11)	H-1→L+4					

[a]Energy (E, in eV), oscillator strength (OS), squared CI coefficients ($c_{\alpha\beta}^2$) of relevant transitions ($c_{\alpha\beta}^2 \geq 0.1$), and the projections of the transition dipole moment (μ, in D) in the GNF plane (xy plane, $\mu_{\parallel}$) and perpendicular to it (z direction, $\mu_{\perp}$). Electron and hole localization on the 7F GNF ($L_{e/h}^{7F}$) and charge transfer character (CT); see text.

covered two different types of stacking, namely, the coupling between identical flakes with different relative displacement (homogeneous stacking) and the coupling between different flakes, carrying different electronic properties in terms of electronic gap or ionization potential (heterogeneous stacking). Our findings indicate that in a disordered ensemble of interacting graphene nanoflakes, with different width and edge termination, a significant increase of the optical absorpion range is to be expected. On the other hand, our analysis of the optical excitations and the transition dipole moments allows us to clarify that one should not expect a considerable enhancement of the absorption intensity. Instead, charge transfer excitonic phenomena relevant in optoelectronic applications can be designed by appropriately choosing the chemical functionalization and the layering procedure.

■ ASSOCIATED CONTENT

Supporting Information

Frontier orbitals for both the homogeneous and the heterogeneous BGNFs that are investigated in this paper; the optical absorption results for additional biflake structures, which are obtained by stacking two 7H flakes wih different relative shifts along their main axis; the details of the UV−vis spectra that are not provided in the main text. This material is available free of charge via the Internet at http://pubs.acs.org.

■ AUTHOR INFORMATION

Corresponding Authors

*M.D.C.: e-mail, marzio.decorato@unimore.it.
*A.R.: e-mail, alice.ruini@unimore.it.

Present Address

[‖]C.C.: Humboldt-Universität zu Berlin, Institut für Physik und IRIS Adlershof, Zum GrossenWindkanal 6, 12489 Berlin, Germany. E-mail: caterina.cocchi@physik.hu-berlin.de.

Notes

The authors declare no competing financial interest.

■ ACKNOWLEDGMENTS

Part of this research was supported by the Italian Ministry of Research through the National Projects PRIN-GRAF (Grant 20105ZZTSE), FIRB-FLASHit (Grant RBFR12SWOJ), and the Program "Progetto Premiale 2012", Project ABNANO-TECH; the Italian Ministry of Foreign Affairs through Grant US14GR12; and the Fondazione Cassa di Risparmio di Modena through the "COLDandFEW" project. M.J.C. acknowledges support from FAPESP and CNPq (Brazil). The authors acknowledge CINECA for computational support.

■ REFERENCES

(1) Smungen, W. *Principles of Nucleic Acid Structure*; Springer-Verlag: New York, 1984; pp 132−140.
(2) Burley, S. K.; Petsko, G. A. Weakly Polar Interactions in Proteins. *Adv. Protein Chem.* **1988**, *39*, 125−192 and references therein.
(3) Meyer, E. A.; Castellano, R. K.; Diederich, F. Interactions with Aromatic Rings in Chemical and Biological Recognition. *Angew. Chem., Int. Ed.* **2003**, *42*, 1210−1250.
(4) Desiraju, G. R.; Gavezzotti, A. From Molecular to Crystal Structure: Polynuclear Aromatic Hydrocarbon. *J. Chem. Soc., Chem. Commun.* **1989**, *10*, 621−623 and references therein.
(5) Watson, M. D.; Fechtenkoetter, A.; Muellen, K. Big Is Beautiful—Aromaticity Revisited from the Viewpoint of Macromolecular and Supramolecular Benzene Chemistry. *Chem. Rev.* **2001**, *101*, 1267−1300.
(6) Hoeben, F. J. M.; Jonkheijm, P.; Meijer, E. W.; Schenning, A. P. H. J. About Supramolecular Assemblies of π-Conjugated Systems. *Chem. Rev.* **2005**, *105*, 1491−1546.
(7) Abraham, R. J.; Eivazi, F.; Pearson, H.; Smith, K. M. π−π Aggregation in Metalloporphyrins: Causative Factors. *J. Chem. Soc., Chem. Commun.* **1976**, 699−701.
(8) Adam, D.; Schuhmacher, P.; Simmerer, J.; Häussling, L.; Siemensmeyer, K.; Etzbachi, K.; Ringsdorf, H.; Haarer, D. Fast Photoconduction in the Highly Ordered Columnar Phase of a Discotic Liquid Crystal. *Nature (London)* **1994**, *371*, 141−143.
(9) Percec, V.; Glodde, M.; Bera, T.; Miura, Y.; Shiyanovskaya, I.; Singer, K.; Balagurusamy, V.; Heiney, P.; Schnell, I.; Rapp, A.; et al. Self-Organization of Supramolecular Helical Dendrimers into Complex Electronic Materials. *Nature (London)* **2002**, *419*, 384−387.
(10) Chen, Z.; Stepanenko, V.; Dehm, V.; Prins, P.; Siebbeles, L. D.; Seibt, J.; Marquetand, P.; Engel, V.; Würthner, F. Photoluminescence and Conductivity of Self-Assembled π−π Stacks of Perylene Bisimide Dyes. *Chem.—Eur. J.* **2007**, *13*, 436−449.
(11) Liu, R.; Wu, D.; Feng, X.; Müllen, K. Bottom-Up Fabrication of Photoluminescent Graphene Quantum Dots with Uniform Morphology. *J. Am. Chem. Soc.* **2011**, *133*, 15221−15223.

(12) Ohta, T.; Bostwick, A.; Seyller, T.; Horn, K.; Rotenberg, E. Controlling the Electronic Structure of Bilayer Graphene. *Science* **2006**, *313*, 951−954.
(13) Zhang, Y.; Tang, T.-T.; Girit, C.; Hao, Z.; Martin, M. C.; Zettl, A.; Crommie, M. F.; Shen, Y. R.; Wang, F. Direct Observation of a Widely Tunable Bandgap in Bilayer Graphene. *Nature (London)* **2009**, *459*, 820−823.
(14) Mak, K. F.; Lui, C. H.; Shan, J.; Heinz, T. F. Observation of an Electric-Field-Induced Band Gap in Bilayer Graphene by Infrared Spectroscopy. *Phys. Rev. Lett.* **2009**, *102*, 256405.
(15) Hass, J.; De Heer, W.; Conrad, E. The Growth and Morphology of Epitaxial Multilayer Graphene. *J. Phys.: Condens. Matter* **2008**, *20*, 323202.
(16) Jiao, L.; Zhang, L.; Wang, X.; Diankov, G.; Dai, H. Narrow Graphene Nanoribbons from Carbon Nanotubes. *Nature (London)* **2009**, *458*, 877.
(17) Kosynkin, D. V.; Higginbotham, A. L.; Sinitskii, A.; Lomeda, J. R.; Dimiev, A.; Price, B. K.; Tour, J. M. Longitudinal Unzipping of Carbon Nanotubes To Form Graphene Nanoribbons. *Nature (London)* **2009**, *458*, 872.
(18) Jiao, L.; Wang, X.; Diankov, G.; Wang, H.; Dai, H. Facile Synthesis of High-Quality Graphene Nanoribbons. *Nat. Nanotechnol.* **2010**, *5*, 321−325.
(19) Barone, V.; Hod, O.; Scuseria, G. E. Electronic Structure and Stability of Semiconducting Graphene Nanoribbons. *Nano Lett.* **2006**, *6*, 2748−2754.
(20) Son, Y.-W.; Cohen, M. L.; Louie, S. G. Energy Gaps in Graphene Nanoribbons. *Phys. Rev. Lett.* **2006**, *97*, 216803.
(21) Pisani, L.; Chan, J. A.; Montanari, B.; Harrison, N. M. Electronic Structure and Magnetic Properties of Graphitic Ribbons. *Phys. Rev. B* **2007**, *75*, 064418.
(22) Prezzi, D.; Varsano, D.; Ruini, A.; Marini, A.; Molinari, E. Optical Properties of Graphene Nanoribbons: The Role of Many-Body Effects. *Phys. Rev. B* **2008**, *77*, 041404(R).
(23) Prezzi, D.; Varsano, D.; Ruini, A.; Molinari, E. Quantum Dot States and Optical Excitations of Edge-Modulated Graphene Nanoribbons. *Phys. Rev. B* **2011**, *84*, 041401.
(24) Yang, L.; Cohen, M.; Louie, S. Excitonic Effects in the Optical Spectra of Graphene Nanoribbons. *Nano Lett.* **2007**, *7*, 3112−3115.
(25) Cocchi, C.; Ruini, A.; Prezzi, D.; Caldas, M. J.; Molinari, E. Designing All-Graphene Nanojunctions by Covalent Functionalization. *J. Phys. Chem. C* **2011**, *115*, 2969−2973.
(26) Genorio, B.; Znidarsic, A. Functionalization of Graphene Nanoribbons. *J. Phys. D: Appl. Phys.* **2014**, *47*, 094012.
(27) Zhu, X.; Su, H. Excitons of Edge and Surface Functionalized Graphene Nanoribbons. *J. Phys. Chem. C* **2010**, *114*, 17257−17262.
(28) Wagner, P.; Ewels, C.; Adjizian, J.-J.; Magaud, L.; Pochet, P.; Roche, S.; Lopez-Bezanilla, A.; Ivanovskaya, V.; Yaya, A.; Rayson, M.; et al. Band Gap Engineering via Edge Functionalisation of Graphene Nanoribbons. *J. Phys. Chem. C* **2013**, *117*, 26790.
(29) Jippo, H.; Ohfuchi, M. First-Principles Study of Edge-Modified Armchair Graphene Nanoribbons. *J. Appl. Phys.* **2013**, *113*, 183715.
(30) Vo, T. H.; Shekhirev, M.; Kunkel, D. A.; Morton, M. D.; Berglund, E.; Kong, L.; Wilson, P. M.; Dowben, P. A.; Enders, A.; Sinitskii, A. Large-Scale Solution Synthesis of Narrow Graphene Nanoribbons. *Nat. Commun.* **2014**, *5*, 3189.
(31) Kharche, N.; Zhou, Y.; O'Brien, K. P.; Kar, S.; Nayak, S. K. Effect of Layer Stacking on the Electronic Structure of Graphene Nanoribbons. *ACS Nano* **2011**, *5*, 6096−6101.
(32) Feng, C.; Lin, C. S.; Fan, W.; Zhang, R. Q.; Van Hove, M. A. Stacking of Polycyclic Aromatic Hydrocarbons as Prototype for Graphene Multilayers, Studied Using Density Functional Theory Augmented with a Dispersion Term. *J. Chem. Phys.* **2009**, *131*, 194702.
(33) Lima, M. P.; Fazzio, A.; da Silva, A. J. R. Edge Effects in Bilayer Graphene Nanoribbons: Ab Initio Total-Energy Density Functional Theory Calculations. *Phys. Rev. B* **2009**, *79*, 153401.
(34) González, J. W.; Santos, H.; Pacheco, M.; Chico, L.; Brey, L. Electronic Transport through Bilayer Graphene Flakes. *Phys. Rev. B* **2010**, *81*, 195406.
(35) Sahu, B.; Min, H.; Banerjee, S. K. Effects of Magnetism and Electric Field on the Energy Gap of Bilayer Graphene Nanoflakes. *Phys. Rev. B* **2010**, *81*, 045414.
(36) Gundra, K.; Shukla, A. Band Structure and Optical Absorption in Multilayer Armchair Graphene Nanoribbons: A Pariser−Parr−Pople Model Study. *Phys. Rev. B* **2011**, *84*, 075442.
(37) Wright, A. R.; Cao, J. C.; Zhang, C. Enhanced Optical Conductivity of Bilayer Graphene Nanoribbons in the Terahertz Regime. *Phys. Rev. Lett.* **2009**, *103*, 207401.
(38) Shemella, P.; Zhang, Y.; Mailman, M.; Ajayan, P.; Nayak, S. Energy Gaps in Zero-Dimensional Graphene Nanoribbons. *Appl. Phys. Lett.* **2007**, *91*, 042101.
(39) Hod, O.; Barone, V.; Scuseria, G. E. Half-Metallic Graphene Nanodots: A Comprehensive First-Principles Theoretical Study. *Phys. Rev. B* **2008**, *77*, 035411.
(40) Nakada, K.; Fujita, M.; Dresselhaus, G.; Dresselhaus, M. S. Edge State in Graphene Ribbons: Nanometer Size Effect and Edge Shape Dependence. *Phys. Rev. B* **1996**, *54*, 17954.
(41) The structures considered here are approximately 24 Å long and less than 10 Å wide.
(42) Ridley, J.; Zerner, M. An Intermediate Neglect of Differential Overlap Techinique for Spectroscopy: Pyrrole and the Azines. *Theor. Chem. Acta* **1973**, *32*, 111−134.
(43) Kwasniewski, S. P.; Deleuze, M. S.; Francois, J. P. Optical Properties of *trans*-Stilbene Using Semi-Empirical and Time-Dependent Density Functional Theory: A Comparative Study. *Int. J. Quantum Chem.* **2000**, *80*, 672.
(44) Lopata, K.; Reslan, R.; Kowalska, M.; Neuhauser, D.; Govind, N.; Kowalski, K. Excited-State Studies of Polyacenes: A Comparative Picture Using EOMCCSD, CR-EOMCCSD(T), Range-Separated (LR/RT)-TDDFT, TD-PM3, and TD-ZINDO. *J. Chem. Theory Comput.* **2011**, *7*, 3686.
(45) Wetmore, S. D.; Boyd, R. J.; Eriksson, L. A. Electron Affinities and Ionization Potentials of Nucleotide Bases. *Chem. Phys. Lett.* **2000**, *322*, 129−135.
(46) Caldas, M. J.; Pettenati, E.; Goldoni, G.; Molinari, E. Tailoring of Light Emission Properties of Functionalized Oligothiophenes. *Appl. Phys. Lett.* **2001**, *79*, 2505−2507.
(47) Dávila, L. Y. A.; Caldas, M. J. Applicability of MNDO Techniques AM1 and PM3 to Ring-Structured Polymers. *J. Comput. Chem.* **2002**, *23*, 1135.
(48) Kubatkin, S.; Danilov, A.; Hjort, M.; Cornil, J.; Brédas, J.; Stuhr-Hansen, N.; Hedegård, P.; Bjørnholm, T. Single-Electron Transistor of a Single Organic Molecule with Access to Several Redox States. *Nature (London)* **2002**, *32*, 567−569.
(49) Machado, A.; Munaro, M.; Martins, T.; Davila, L.; Giro, R.; Caldas, M.; Atvars, T.; Akcelrud, L. Photoluminescence Studies of Phenanthrene−Azomethyne Conjugated−Nonconjugated Multiblock Copolymer. *Macromolecules* **2006**, *39*, 3398−3407.
(50) Dewar, M. J. S.; Zoebish, E. G.; Healy, E. F.; Stewart, J. J. P. A New General Purpose Quantum Mechanical Molecular Model. *J. Am. Chem. Soc.* **1985**, *107*, 3902−3909.
(51) Perdew, J. P.; Burke, K.; Ernzerhof, M. Generalized Gradient Approximation Made Simple. *Phys. Rev. Lett.* **1996**, *77*, 3865−3868.
(52) Grimme, S. Semiempirical GGA-Type Density Functional Constructed with a Long-Range Dispersion Correction. *J. Comput. Chem.* **2006**, *27*, 1787−1799.
(53) Giannozzi, P.; Baroni, S.; Bonini, N.; Calandra, M.; Car, R.; Cavazzoni, C.; Ceresoli, D.; Charotti, G. L.; Cococcioni, M.; Dabo, I.; et al. Quantum ESPRESSO: A Modular and Open-Source Software Project for Quantum Simulations of Materials. *J. Phys.: Condens. Matter* **2009**, *21*, 395502. See also http://www.quantum-espresso.org.
(54) Barone, V.; Casarin, M.; Forrer, D.; Pavone, M.; Sambi, M.; Vittadini, A. Role and Effective Treatment of Dispersive Forces in Materials: Polyethylene and Graphite Crystals as Test Cases. *J. Comput. Chem.* **2009**, *30*, 934−939.
(55) By comparing PBE-D2 and AM1 optimized geometries for the single GNFs, we find small differences in bond lengths (the largest

difference being 0.025 Å) that induce a slight lowering of optical excitation energies,[60] which however does not affect the overall results.
(56) ZINDO/S calculations are performed using a LCAO basis set, the INDO/1 Hamiltonian, and the Mataga−Nishimoto scheme to evaluate Coulomb integrals, as implemented in the VAMP module included in the Accelrys Materials Studio software, version 6.0 (http://accelrys.com/products/materials-studio). The validation of the ZINDO scheme with respect to ab initio approaches was presented in many previous works (e.g., see refs 43 and 44), while it was discussed in ref 62 for the specific graphene flakes addressed here.
(57) Cocchi, C.; Prezzi, D.; Ruini, A.; Caldas, M.; Molinari, E. Optical Properties and Charge-Transfer Excitations in Edge-Functionalized All-Graphene Nanojunctions. *J. Phys. Chem. Lett.* **2011**, *2*, 1315−1319.
(58) Jensen, F. *Introduction to Computational Chemistry*, 2nd ed.; Wiley: Hoboken, NJ, 2007.
(59) Sahu, B.; Min, H.; MacDonald, A. H.; Banerjee, S. K. Energy Gaps, Magnetism, and Electric-Field Effects in Bilayer Graphene Nanoribbons. *Phys. Rev. B* **2008**, *78*, 045404.
(60) Cocchi, C.; Prezzi, D.; Ruini, A.; Caldas, M. J.; Molinari, E. Electronics and Optics of Graphene Nanoflakes: Edge Functionalization and Structural Distortions. *J. Phys. Chem. C* **2012**, *116*, 17328−17335.
(61) Milko, M.; Puschnig, P.; Blondeau, P.; Menna, E.; Gao, J.; Loi, M. A.; Draxl, C. Evidence of Hybrid Excitons in Weakly Interacting Nanopeapods. *J. Phys. Chem. Lett.* **2013**, *4*, 2664−2667.
(62) Cocchi, C.; Prezzi, D.; Ruini, A.; Benassi, E.; Caldas, M. J.; Corni, S.; Molinari, E. Optical Excitations and Field Enhancement in Short Graphene Nanoribbons. *J. Phys. Chem. Lett.* **2012**, *3*, 924−929.